Seismic Responses Analysis of Suspended Ceiling Structure Attached to Large LNG Storage Tank

Yu Fu(✉), Jiuhuan Cheng, and Juan Su

Offshore Oil Engineering Co., Ltd, Tianjin 300461, NJ, China
fuyu1_cumtb@163.com

Abstract. The suspended ceiling (SC) of LNG storage tank on land is mainly composed of hanger rods, reinforcing rings, and aluminum panels. The hanger rods are prone to damage during earthquakes, which will affect the safe operation of the whole storage tank. In order to facilitate the study of the response of the SC under horizontal seismic shaking, the finite element models of the hanger rods with four different sections, including rectangular, circular, thin-walled circular tube, and groove shape, were established using the ABAQUS software. By inputting EL-Centro horizontal seismic waves, the dynamic time-history analysis is carried out for four hanger rod models with different sections. The response characteristics of acceleration, displacement and internal force with time are obtained, and the comparative analysis results of the maximum peak acceleration (MPA), maximum peak displacement (MPD), and maximum peak internal force (MPIF) at each measuring point are obtained. The results show that the shape of the section has obvious influence on the seismic response of the hanger rods, and the amplitudes of the acceleration-time and displacement-time curves of the hanger rods with different sections are different, and the MPA, MPD and MPIF of the hanger rods are closely related to the shape of the section.

Keywords: LNG · Storage Tank · Suspended Ceiling · Finite Element · Seismic Response

1 Introduction

As a clean energy source, LNG will account for a significant increase in the future energy consumption structure. In the entire industrial chain, LNG storage and transportation are very important link. With the development of technology, the storage tank volume is increasing, and the safe operation and maintenance of LNG storage tanks have become the focus and difficulty. As important energy infrastructure, large-scale LNG storage tanks also have profound significance for national economic construction and energy security. The SC is an important part of the insulation structure of onshore LNG storage tank, which affects the evaporation rate of the storage tank during operation. At the same time, the SC, a kind of suspended structure, is located in the internal space of the storage tank. Under the horizontal earthquake shaking, the hanger rods need to bear various

© The Author(s) 2024
G. Feng (Ed.): ICCE 2023, LNCE 526, pp. 200–212, 2024.
https://doi.org/10.1007/978-981-97-4355-1_19

forces, resulting in large deformation of the structure. Once the structural unsafe factors occur during operation, the tank should be shut down for maintenance, which will cause great economic losses and affects the safety of other structures, such as the inner tank [1].

Scholars have studied the seismic performance and dynamic response of the SC through experimental researches and numerical simulations. Soroushian et al. [2] summarized the damage phenomena of suspended ceilings in three shaking table tests conducted by the University at Buffalo, University of Nevada, Reno, and the Earthquake Engineering Research Center of Japan. Yao et al. [3] studied the impact of the installation of lateral supports on the seismic performance and seismic response of suspension structures by using multidimensional shaking table test method. Takhirov et al. [4] proposed a method for reinforcing the connection between the SC system boundary and a new seismic clamping structure based on the boundary damage characteristics of the SC system. Zaghi et al. [5–7] established five common damage models of suspended ceilings based on OpenSEES, and analyzed their damage evolution process. Kou Miaomiao [8] and Zhang Peng et al. [9] established a simplified analytical model of suspended ceilings based on ANSYS, and took the response spectrum of the floor of the three-story frame structure obtained from the time-history analysis as an incentive to study the law of the influence of the installation of the cable and the floor height on the seismic response of the continuous SC.

It can be seen that there are more studies on the SC structure of traditional buildings at present, but there are fewer studies on the SC of special building structures, such as LNG storage tanks. In this paper, the SC structure of a 200,000 m^3 LNG storage tank is taken as the research object. Based on finite element simulation analysis, the dynamic response characteristics of the acceleration, displacement and internal force of the hanger rods with four kinds of cross-sections under horizontal earthquake are studied, and the differences in the seismic response results of hanger rods with different sections are compared and analyzed. The research in this paper can provide help for the optimization of SC design and the improvement of seismic performance in storage tank engineering.

2 Composition of SC System

The top of the inner tank of the onshore LNG storage tank is open, and the SC structure is located at the top of the inner tank, which is composed of hanger rods, reinforcing rings, and aluminum panels. The detailed structure is shown in Fig. 1. The LNG storage tank is insulated mainly by covering the SC with elastic felt, and the SC function is to provide support for the insulation layer. This design can reduce the heat exchange between the internal low-temperature medium and the external environment, so as to achieve thermal insulation. In order to make the cold protection effect better, a thicker cold insulation layer needs to be laid, which requires the SC to bear more weight. At the same time, the SC also needs to bear its own weight and other live load.

Figure 2 shows the relevant design parameters of the 200,000 m^3 LNG storage tank SC. The radius of the SC reaches 40.4 m, and the aluminum panels of the SC are all made of 5 mm thick slabs in a certain sequence, and a sealed overall structure is formed

by welding at the overlapping place. As a connection between the dome and the SC, the current design of the hanger rod is a 304L flat steel rod with a cross-section size of 50 mm × 8 mm. The number and length of the steel rod in each ring are different, but in order to balance the force, the length of the same ring of steel rod is the same. There are a total of 12 rings of the hanger rods, and the length of the hanger rods from the center ring to the outer ring gradually becomes shorter. The connector at the bottom of each flat steel rod is connected to the reinforcing ring of the SC by bolts. The reinforcing ring on the aluminum plate of the SC is vertically arranged (i.e. the long side direction of the section is along the vertical direction). All the reinforcing rings are concentric circles with the radius from R1 to R12. There are 12 rings of reinforcing ring in total, which are vertically welded on the aluminum plate by flat material. The thickness of the middle reinforcing ring (vertical) is 18 mm, and the most outer reinforcing ring is welded into a T-shape by flat aluminum with a thickness of 30 mm.

In this paper, four kinds of hanger rods with the same cross-section area and different cross-section shapes are designed. The cross-sectional areas are all 400 mm^2, and the sections are rectangular, thin-walled circular tube and groove shape respectively. All the materials and lengths are the same. In order to determine the difference between the same area and different sectional shapes of the hanger rods, the moments of resistance and section modulus of the hanger rods are calculated according to the theoretical formula. The calculation results show that the moment of inertia of thin-walled circular tube section is the largest, the section modulu of groove section is the largest, as shown in Table 1.

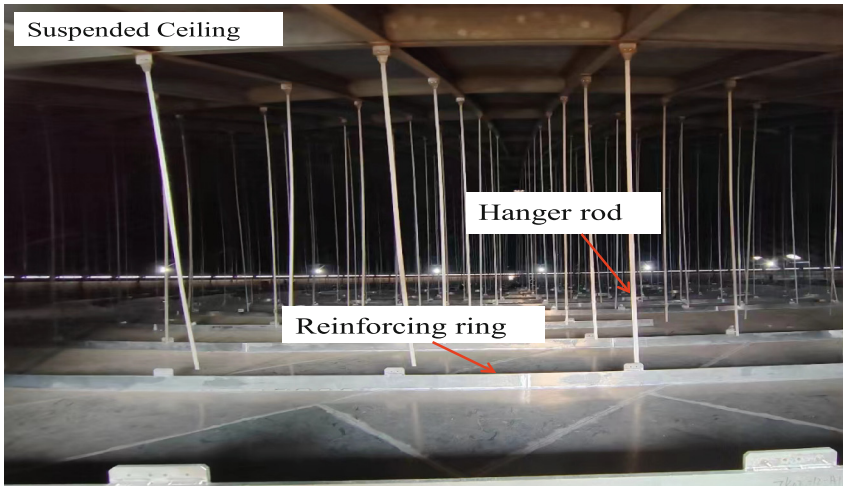

Fig. 1. Suspended ceiling

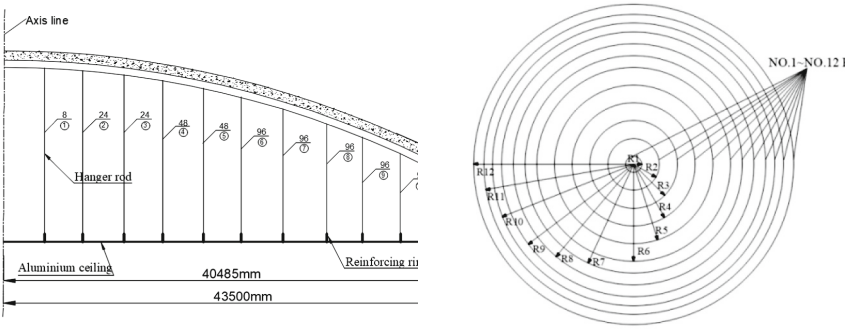

(a) Section view of the ceiling (b) Reinforcing ring layout of the SC

Fig. 2. Schematic diagram of SC

Table 1. Parameters of cross-section

Number	Sectional shape	Sectional area (mm^2)	Moment of inertia (× 104 mm^4)	Moment of resistance (× 103 m^3)
Section1	Rectangle	400	0.213	0.533
Section2	Circle	400	1.272	1.127
Section3	Thin-walled circular tube	400	3.867	2.417
Section4	Grooved	400	3.739	2.460

3 Analysis Model of SC

3.1 Finite Element Model

Three-dimensional finite element analysis models of hanger rod with four kinds of sections were established by finite element software ABAQUS, as shown in Fig. 3. The actual shape of the structure was taken into account to ensure the accuracy of the calculation results, and the model was simplified as far as possible to improve the calculation efficiency. In the model, the beam element model is used for the hanger rod and reinforcing ring, and the shell element is used for the aluminum plate. Then the section properties are set according to their respective characteristics to complete the setting of various material parameters, and the section direction of the beam element is set by rotating method. In the model, the aluminum plate and the reinforcing ring of the SC adopt a common node, so that the beam and the shell are overlapped. In the process of modeling, the hanger rod model is established separately, and then it is bound to the reinforced ring model as a whole by the combination method.

The present test results show that reinforcing ring (tee) and hanger rod basically maintain elastic state under earthquake shaking, and elastic beam element is used in the

model [10]. In the simulation, the top of the hanger rod is simplified as a fixed. A rigid connection is arranged between the bottom of the hanger rod and the reinforcing ring [11].

When setting the boundary conditions required for the model, the main considerations are displacement boundaries and loads. The main permanent load in the SC is the self-weight of the structure, which mainly includes the self-weight of the hanger rod, aluminum panel, and reinforcement ring, as well as some connecting components. However, compared to the self-weight of the structure, this part of the structural weight can be ignored. In addition to its own weight, another important load is the insulation load laid on the SC. Due to the uniform distribution of the insulation layer, the total weight of the insulation structure can be calculated based on the actual thickness and density of the insulation load. Then, the average load is obtained by dividing the weight by the area, and then applied to the upper surface of the SC in a uniform load manner.

When setting the boundary conditions of the model, the load should be considered in addition to the displacement boundary. The permanent load on the SC is the self-weight of the structure, which mainly includes the weight of the hanger rods, aluminum panels and reinforced rings, and also includes some other connecting screw. But compared with the structural self-weight, the weight of the connecting screw can be ignored. In addition to its self-weight, another main load is the weight of the insulation material laid on the SC. Because the insulation layer is uniform distribution, the total weight of the insulation layer can be calculated according to the actual thickness and density, and then the value of the average load is calculated. Finally, it is applied as a uniformly distributed load on the upper surface of the SC.

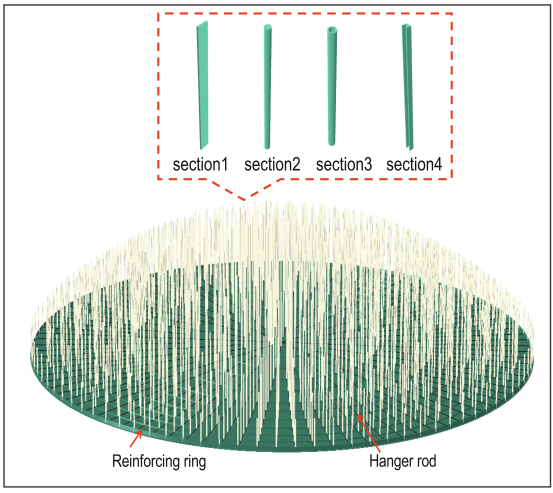

Fig. 3. Finite element model of SC

3.2 Measuring Points

According to the symmetry characteristics of the model, the measuring points are arranged in the X direction parallel to the seismic action and the Y direction perpendicular to the seismic action. A total of five measuring points from A1 to A5 are arranged in the X direction, and the same number of measuring points from B1 to B5 are also arranged in the Y direction. Measuring point A1 is located on the ring of hanger rod nearest to the center, measuring point A5 is located on the ring of hanger rod farthest from the center, and A2, A3 and A4 are located the 2nd, 4th and 6th rings where the number of hanger rod changes, respectively. There are a total of 10 measuring points, and their specific layout is shown in Fig. 4(a). The corresponding hanger rods and its position are shown in Fig. 4(b).These measuring points were used to record the dynamic response of SC structure under seismic loading and obtain the corresponding dynamic characteristics.

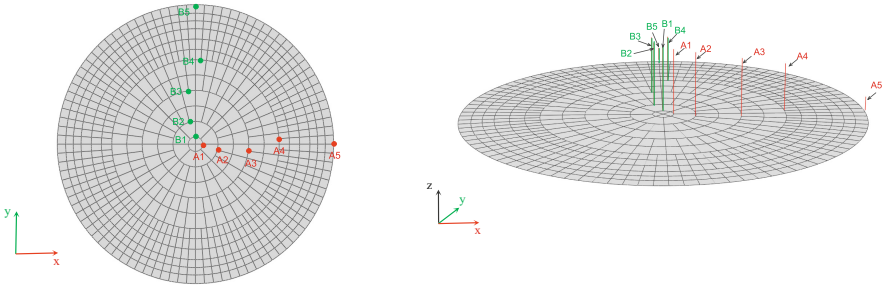

(a) Measuring points

(b) The hanger rod corresponding to the measuring point

Fig. 4. Measuring points layout

3.3 Damping

In general, structural damping should be considered in the analysis of structural dynamic characteristics. In this paper, Rayleigh damping system is adopted for the time-history analysis of the SC. The two proportional coefficients of damping are calculated according to Formula (1)–(3) [12], and the damping ratio of structural vibration mode is 5% [13]. Damping can be calculated by the following formula.

$$C = \alpha[M] + \beta[N] \tag{1}$$

$$\alpha = \xi \frac{2\omega_1\omega_2}{\omega_1 + \omega_2} \tag{2}$$

$$\beta = \frac{2\xi}{\omega_1 + \omega_2} \tag{3}$$

where α and β are two proportional coefficients, with dimensions of s^{-1} and s, respectively; ξ is damping ratio; and ω_1, ω_2 are the fundamental natural frequencies of the SC in X direction and Y direction respectively.

Based on the principle that the selected two natural frequencies should include the frequency that has a great influence on the structural response, the 1st natural frequency and the 10th natural frequency are selected to calculate Rayleigh damping. The calculation results are shown in Table 2.

Table 2. Rayleigh damping coefficient

Number	ω_1	ω_{10}	α	β
Section1	0.2445	0.2530	0.0781	0.0320
Section2	0.2281	0.5974	0.1037	0.0193
Section3	0.3806	1.0158	0.1739	0.0114
Section4	0.3470	0.6845	0.1446	0.0154

3.4 Materials Properties

According to ASTM B209M specification [14], the material of the aluminum panels is B209 5083-O, and the reinforcing rings are the same material as the aluminum panels. The material of the hanger rods is A276Gr 304L stainless steel, which bears the main load transfer function. The constitutive relation of hanger rod, reinforcing ring and aluminum plate is only considered elasticity. At the same time, it is necessary to consider the large deformation of the aluminum ceiling, so the large deformation switch should be set to open when determining the material properties. The material parameters of the finite element model of the SC structure are shown in Table 3.

Table 3. Material information

Ceiling component	Material	Density (kg·m^{-3})	Elastic Modulus (MPa)	Poisson ratio
Hanger rod	A276Gr 304L	7850	2 × 105	0.3
Reinforcing ring	B209 5083-O	2710	78000	0.34
Aluminum panels	B209 5083-O	2710	78000	0.34

4 The Selection of Seismic Waves

In this paper, the time-history analysis method is selected to analyze dynamic response of SC structure. According to the regulations, when the dynamic time-history analysis of the structure is carried out, acceleration time-history curves of the actual strong earthquake records and artificial simulated should be selected according to the classification of building site and the design earthquake groups, and the number of actual strong earthquake records should not be less than 2/3 of the total [15]. This paper only takes a real seismic wave as an example to analyze and illustrate, and some representative nodes' displacement and rods' dynamic inner force are given, as the amount of data of results of the dynamic analysis is so great. The seismic wave used for calculation and analysis in this paper is EL-Centro wave, and the time-history curve of the seismic wave is shown in Fig. 5. The peak acceleration of EL-Centro wave is 342 cm/s^2, and the duration is taken as 30 s.

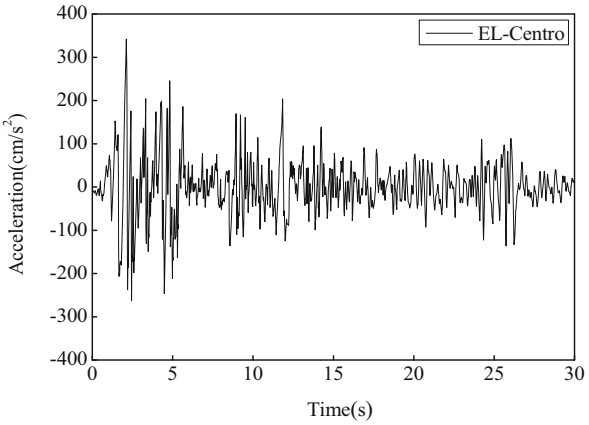

Fig. 5. Acceleration time history of ground motions

5 Response Analysis and Discussion

5.1 Acceleration Response

The relative acceleration response of each measuring point can be obtained through the acceleration time-history data. The MPA of each measuring point can be calculated using by Formula 4:

$$A_j = max\{|a_i(t)|\} \tag{4}$$

$a_i(t)$ is the acceleration time-history of different measuring points of the model, A_j is the MPA corresponding to each measurement point.

Figure 6(a) and (b) compare the MPA of four hanger rod models with different sections. It can be seen that the magnitude relation of the MPA of the hanger rod models

are as follows: Section 4 > Section 3 > Section 1 > Section 2, indicating that the section shape of the hanger rod affects the MPA of the structure under earthquake load. In Fig. 6(a), the acceleration response of the A5 measuring point of the hanger rod at the most outer ring is more obvious than that at other positions in the parallel seismic input direction. Compared with the initial input acceleration, the MPA of the models corresponding to Section 1, Section 2, Section 3 and Section 4 increase by 141%, 46.5%, 154% and 189% respectively.

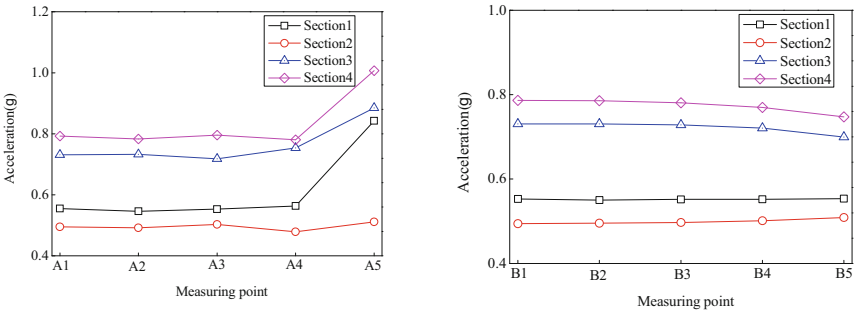

(a) A1~A5 (b) B1~B5

Fig. 6. Comparison of maximum peak acceleration (MPA)

5.2 Displacement Response

The MPD of each measuring point of the model is also calculated according to the method of formula (4). Figure 7(a)–7(b) shows the comparison of the MPD of four types of cross-sectional hanger rod models at different measuring points. It can be seen that the displacement response of Section 2 is obviously smaller than the other three sections. The relationship between the MPD of each measuring points of the four sectional hanger rod models is: Section 3 > Section 4 > Section 1 > Section 2. However, the peak displacement response of the same section at each measuring point is basically the same, indicating that the maximum displacement difference between each ring of the hanger rods is very small.

5.3 Internal Force Response

The failure of the hanger rod connection point is an important feature of the SC failure, and the magnitude of the hanger rod axial force is an important cause of the failure of the SC connection point. Figure 8 shows the maximum peak axial force (MPAF) of the hanger rods corresponding to each measuring point. It can be seen that in measuring points A1–-A4 and B1–B3, the MPAF of the hanger rod corresponding to Section 1 is greater than that of other sections. The MPAF increases significantly at measuring points A5 and B5, indicating that the axial force on the most outer ring hanger rod is subjected to the largest axial force and the axial force response under seismic action

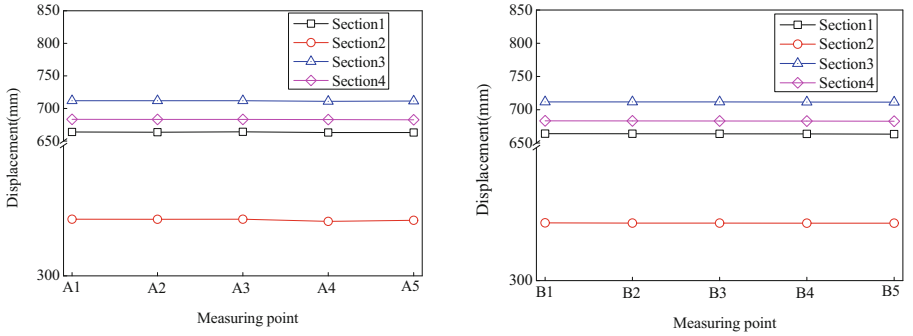

(a) A1~A5 (b) B1~B5

Fig. 7. Comparison of maximum peak displacement (MPD)

is more obvious. The difference in the MPAF of the hanger rod with different section forms indicates that although the section area is the same, the combined action of the axial force and bending moment on each hanger rod will affect the final axial force.

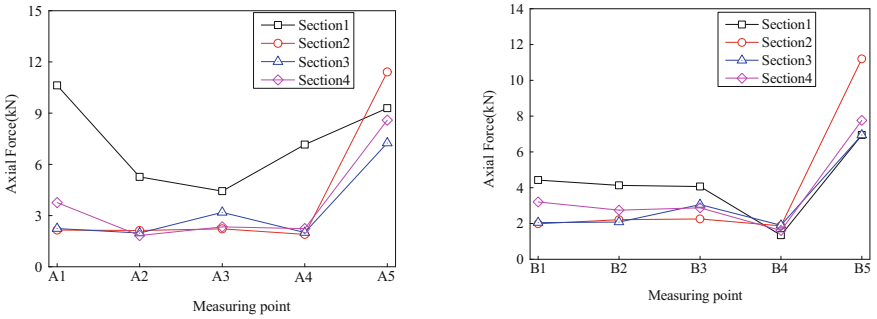

(a)A1~A5 (b)B1~B5

Fig. 8. Comparison of maximum peak axial force (MPAF)

Figure 9 compares the maximum peak bending moments (MPBM) of the hanger rod models with different cross-section at each measuring point. It can be seen from Fig. 9(a) that the MPBM corresponding to different cross-sections at A1 –A5 measuring points are: Section 3 > Section 4 > Section 2 > Section 1. The maximum bending moment appears at A5 measuring point, and the MPBM of the hanger rods with four sections increases significantly, indicating that the most outer ring hanger rod bears greater bending moment in the direction of seismic wave input. Figure 9(b) shows the comparison of the MPBM of the hanger rods from B1 to B5. It can be seen that the maximum value of the hanger rod with Section 1 occurs at B1 measurement point, while the maximum values of Section 2, Section 3, and Section 4 occur at B2 measurement point. It can be seen from Table 2 that the moment of inertia and moment of resistance of the hanger rod in different sections are different, resulting in the difference in the bending

moment of the hanger rod with the corresponding section. In addition, the magnitudes of the inertia moments of asymmetric cross-sections in different directions are not equal, so when the direction of force action changes, the bending moment of the hanger will exhibit differences.

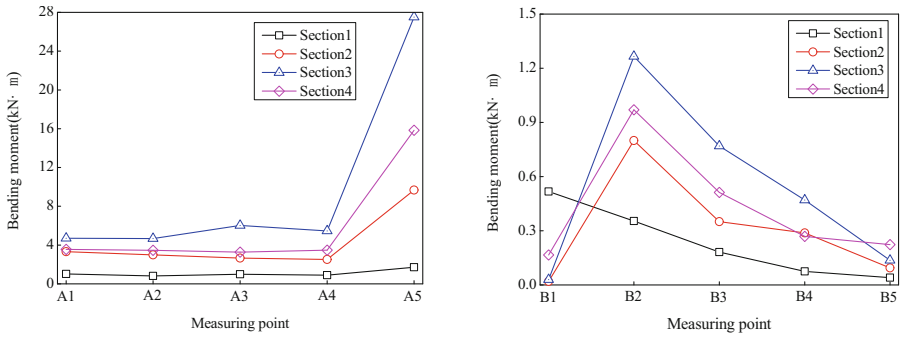

(a) A1~A5 (b) B1~B5

Fig. 9. Comparison of maximum peak moment

6 Conclusions

The safety of the suspender structure under earthquake action is very important for the overall safety of the LNG storage tank structure. Through the simulation calculation of four different cross-section suspender models including rectangular, circular, thin-walled circular tube, and groove shape under horizontal earthquake action, and the comparative analysis of the displacement, acceleration, and internal force of the SC structure, the following conclusions are obtained.

(1) Through the comparative analysis of displacement-time curve and peak acceleration, it is found that the peak acceleration responses of four kinds of hanger rods with different cross-sections are different. The acceleration response of the hanger rod is affected by the cross-sectional form of the hanger rod. Compared with the initial input acceleration ratio, the MPA of the models corresponding to rectangular cross-Section 1, circular cross-Section 2, thin-walled circular tube cross-Section 3, and groove-shaped cross-Section 4 increased by 141%, 46.5%, 154%, and 189%, respectively.

(2) The MPD of the hanger rod under seismic action is significantly affected by the sectional form of the hanger rod. The MPD of the hanger rod in the same section at different measuring points are very close. The relationship between the MPD of the four sections is: thin-walled circular tube > groove shape > rectangular > circular.

(3) The internal force response of the hanger rod under earthquake action is an important factor affecting the structural safety. The moment of inertia and resistance moment of different sections of the hanger rod are different. Under horizontal earthquake

action, the MPIF of the hanger rod with different sections is significantly different, and the MFIF of the most outer ring of the hanger rod is greater in the direction parallel to the earthquake action.

References

1. Zhai, X., Zhao, X., Wang, Y.: Numerical modeling and dynamic response of 160,000–m^3 liquefied natural gas outer tank under aircraft impact. J. Perform. Constr. Facil. **33**(4), 04019039 (2019)
2. Soroushian, S., Rahmanishamsi, E., Ryu, K.P., Maragakis, E.M., Reinhorn, A.M.: A comparative study of sub-system and system level experiments of suspension ceiling systems. In: Proceedings of the 10th US National Conference on Earthquake Engineering Frontiers of Earthquake Engineering, July 2014
3. Yao, G.C., Chen, W.C.: Vertical motion effects on suspended ceilings. In: Proceedings of the 16th World Conference on Earthquake Engineering, January 2017
4. Takhirov, S.M., Gilani, A.S., Straight, Y.: Seismic evaluation of lay-in panel suspended ceilings using static and dynamic and an assessment of the US building code requirements. In: Improving the Seismic Performance of Existing Buildings and Other Structures 2015, pp. 483–496 (2015)
5. Soroushian, S., Maragakis, E.M., Jenkins, C.: Capacity evaluation of suspended ceiling components, part 1: experimental studies. J. Earthq. Eng. **19**(5), 784–804 (2015)
6. Soroushian, S., Maragakis, M., Jenkins, C.: Axial capacity evaluation for typical suspended ceiling joints. Earthq. Spectra **32**(1), 547–565 (2016)
7. Zaghi, A., Soroushian, S., Echevarria Heiser, A., Maragakis, M., Bagtzoglou, A.: Development and validation of a numerical model for suspended-ceiling systems with acoustic tiles. J. Archit. Eng. **22**(3), 04016008 (2016)
8. Miaomaio, K.: Research on Seismic Performance of Nonstructural Components. Tianjin University, Tianjin (2014). (in Chinese)
9. Zhang, P., Lu, Y.: Seismic response analysis of suspended ceiling in frame structure. In: Tianjin University and Tianjin Steel Structure Association. Proceedings of the 14th National Symposium on Modern Structural Engineering, pp. 1467–1473 (2014). (in Chinese)
10. Jiang, H., Wang, Y., He, L.: Study of seismic performance of Chinese-style single-layer suspended ceiling system by shaking table tests. Adv. Civ. Eng. **2021**, 1–14 (2021)
11. Jun, S.C., Lee, C.H., Bae, C.J., Lee, K.J.: Shake-table seismic performance evaluation of direct-and indirect-hung suspended ceiling systems. J. Earthq. Eng. **26**(9), 4833–4851 (2022)
12. Jiang, H., Huang, Y., He, L., Wang, Y., Wang, H.: Numerical modeling and experimental validation for suspended ceiling system with free boundary condition. J. Build. Eng. **61**, 105285 (2022)
13. Anajafi, H., Medina, R.A., Santini-Bell, E.: Inelastic floor spectra for designing anchored acceleration-sensitive nonstructural components. Bull. Earthq. Eng. **18**(5), 2115–2147 (2020)
14. ASTM B Standard: Standard Specification for Aluminum and Aluminum-Alloy Sheet and Plate (2014)
15. Ministry of Housing and Urban-Rural Development of the People's Republic of China: Code for Seismic Design of Buildings: GB 50011-2010. 2016 ed. China Architecture & Building Press, Beijing (2016). (in Chinese)

Open Access This chapter is licensed under the terms of the Creative Commons Attribution 4.0 International License (http://creativecommons.org/licenses/by/4.0/), which permits use, sharing, adaptation, distribution and reproduction in any medium or format, as long as you give appropriate credit to the original author(s) and the source, provide a link to the Creative Commons license and indicate if changes were made.

The images or other third party material in this chapter are included in the chapter's Creative Commons license, unless indicated otherwise in a credit line to the material. If material is not included in the chapter's Creative Commons license and your intended use is not permitted by statutory regulation or exceeds the permitted use, you will need to obtain permission directly from the copyright holder.